DOI: 10.31276/VJSTE.62(4).87-94

Application of remote sensing in evaluating the PM_{10} concentration in Ho Chi Minh city

Tran Huynh Duy[1], Duong Thi Thuy Nga[2*]

[1]University of Science, Vietnam National University, Ho Chi Minh city
[2]Ho Chi Minh city University of Natural Resources and Environment

Received 12 August 2020; accepted 9 November 2020

Abstract:

Nowadays, air pollution is a serious problem for the entire world, but especially in developing countries like Vietnam. For monitoring and managing air quality, scientists have successfully used different technologies such as predictive models, interpolation, and monitoring, however; these methods require a large amount of input data to simulate. Further, the results from spatial simulations are not detailed and have deviations from reality due to factors such as terrain changes, wind direction, and rainfall. Based on the physical index extracted from remote sensing images like radiation and reflection values, the aerosol optical depth (AOD) can be extracted. In this work, a regression equation is constructed and the correlation between the extracted AOD and measured PM_{10} concentration is found. The results show that PM_{10} and AOD are best correlated with a non-linear regression equation. This work also shows that the concentration of PM_{10} in Ho Chi Minh city is distributed mainly along the outskirts of the city, which has many highways, industrial parks, factories, and enterprises.

Keywords: **AOD, Ho Chi Minh city, Landsat, PM_{10}.**

Classification number: **5.1**

Introduction

In recent years, countries around the world, along with Vietnam in particular, have been developing, urbanising, and modernising. What has followed is the emergence of many factories and means of transportation. As a result, the emission of dust and pollutants into the environment are increasing.

The National Environmental Status Report 2016 advises that most major cities in Vietnam are facing increasing air pollution [1]. Pollution levels among cities vary widely depending on urban size, population density, traffic density, and construction speed. As for dust pollution, data observed from 2012 to 2016 showed that dust pollution levels in urban areas are high with no sign of reduction over the last 5 years. For PM_{10} and $PM_{2.5}$ dust alone, the measured values at many traffic stations are higher than the annual average threshold, which was mentioned in QCVN 05:2013/BTNMT. According to the 2015 WHO Report, there are 6 diseases related to the respiratory tract that are caused by air pollution and these 6 are among the top 10 diseases with the highest mortality rates in Vietnam. In Vietnam, respiratory diseases are also one of the 5 most prevalent groups of acquired diseases [2, 3].

In order to prevent and minimise the level of pollution, the country has been the subject of a lot of studies that evaluate the air pollution level using the AQI index that is made up of the concentration of pollutant gases of CO_2, VOCs, and NO_x in many urban areas. Nevertheless, these studies only focus on processing data available from ground observation stations for simulation and prediction. These results have some deviations from reality due to the influence of many different factors such as the density of monitoring stations, the terrain where the stations are located, etc. In addition, some studies use modelling but are limited due to the need for a large enough input data source to get simulation results.

Because of these shortcomings, remote sensing is put into use. Remote sensing images show topographical and

*Corresponding author: Email: ngadtt@gmail.com

spatial information of the study area through pixels. Each pixel represents a monitoring station and the concentration of PM_{10} in the area will be more detailed compared to data taken by monitoring stations on the ground. At that time, each pixel will have a specific concentration value, which can show us a general view and clearer distribution of the fine dust in Ho Chi Minh city.

Up to now, Vietnam has had only a few studies using remote sensing technology for monitoring air pollution concentrations in the region. Tran Thi Van, et al. (2014) [4] with the study "Remote sensing aerosol optical thickness (AOT) simulating PM_{10} in Ho Chi Minh city area" used satellite images from Landsat 7 to develop the AOD index in 2003 based on "a clean image" from 1996. Then, the study had given the correlation equation between the real measured AOD and PM_{10}. A similar study was conducted by Nguyen Nhu Hung, et al. (2018) [5] in the Hanoi area titled "Model to determine PM_{10} in Hanoi area using Landsat 8 OLI satellite image data and visual data". Both studies provided a PM_{10} simulation map in two areas at the time of the study, but only at the correlation assessment at the 1-year level. With the same method, this study, which used correlation equations of 1 year for different years of the same period (same February of all years), showed the feasibility of applying remote sensing in simulating air pollution in the area.

Materials and methods

The basic principle of remote sensing technology is based on the reflection and radiation energy of the electromagnetic waves of objects. Different observations on objects will have different reflections at different electromagnetic wavelengths.

Spectral reflection of natural objects

Different observation objects will have various reflection characteristics for different electromagnetic wavelengths. It can be seen in some typical objects, for example, water reflection mainly ranges around 0.4-0.7 μm and is strongly reflected in the blue wavelength (0.4-0.5 μm) and green (0.5-0.6 μm) regions or soil objects whose reflection increases gradually with wavelength. Based on this characteristic, data can be extracted using remote sensing images [6] (Fig. 1).

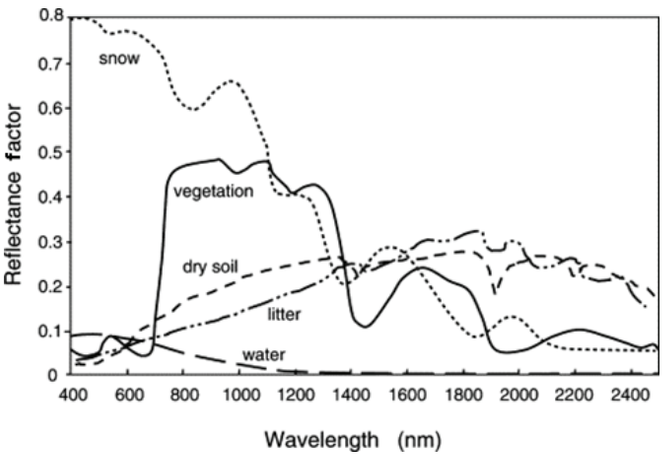

Fig. 1. Spectral reflection of common objects [6].

There are many ways to extract information from remote sensing images in the reflectance spectrum such as visual interpretation or digital image processing. The basis for visual interpretation is direct reading signs. Digital image processing aims to extract information with the help of a computer and is based on the digital signals of pixels. Both methods have different advantages and disadvantages and are applied depending on the purpose.

AOD/AOT

Aerosols are a collection of suspended substances dispersed in air. Aerosols can be in solid or liquid form or in the form of a colloid, which is relatively durable but difficult to deposit. An aerosol system consists of a particle and the air mass containing it. Aerosols can be produced through mechanical decomposition on land or sea (such as sea dust) and by chemical reactions that take place in the atmosphere (such as converting SO_2 to H_2SO_4 in the atmosphere). Moreover, they are also discharged directly into the atmosphere through human daily activities. Natural aerosols include fog, forest secretions, and geysers [7].

When solar radiation enters the atmosphere, some will be lost due to absorption and scattering of material components in the atmosphere, which includes aerosols. To characterise the attenuation of the solar radiation when absorbed and scattered by aerosols, the AOD/AOT is used. According to previous studies, to estimate atmospheric depletion, the moon was used as a source of radiation to calculate the atmospheric emission by the function:

$$T = e^{\frac{-\beta l}{\cos\theta}} \quad (1)$$

where T is the atmospheric transmittance, β is the optical index of the surveyed material, l is the atmospheric thickness, and θ is the angle of the main projection ray measured from the zenith [8]. The transmittance of the atmosphere ranges from 0 to 1, where 0 corresponds to a completely opaque

atmosphere and 1 corresponds to a completely transparent atmosphere. According to the functions, the optical thickness (OT) is inversely proportional to atmospheric emission. A large OT means transmittance through the atmosphere is low and OT also has a value ranging from 0 to 1. However, a 0 value for OT corresponds to a completely transparent atmosphere while a value of 1 corresponds to an atmosphere that is completely opaque.

Implementation steps and research methods (Fig. 2)

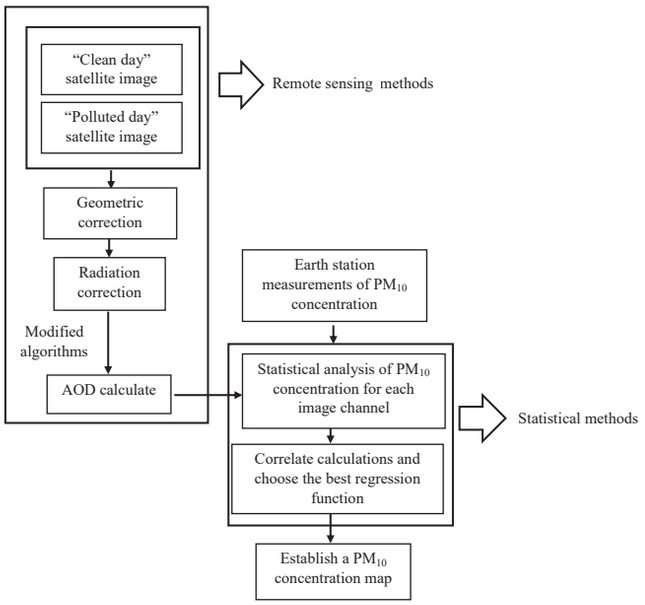

Fig. 2. Implementation steps and research methods [8].

Geometric correction

Before analysis and interpretation, satellite images must be corrected geometrically to limit position errors and terrain differences, which makes it easier to analyse and detect changes. In addition, geometric corrections are also carried out to eliminate distortions during photography and to return images to standard coordinates so that they can be integrated with other data sources. To perform the geometric correction, the authors select ground control points (GCPs). The coordinate parameters are included in the least-squares regression analysis to determine the coefficients of the conversion equation between images and map coordinates. After the conversion equation, the sample redistribution process is performed to determine the pixel values included in the corrected image. The interpolation methods that are applied in the re-division process are interpolation and tertiary interpolation. In order to retain the spatial and radiation quality of the image, the nearest neighbour interpolation method is used over the whole course of image processing.

Radiation correction [9-13]

Conversion to radiation values: this study uses remote sensing images from Landsat 5 TM (used as "clean day" images) and Landsat 8 (for the time of observation).

For the Landsat 5 TM:

$$L_\lambda = A \times (DN - Q_{min}) + B \quad (2)$$

where L_λ is the radiation value on the satellite ($Wm^{-2}\mu m^{-1}$), Q_{min} is the minimum quantitative reflection value on the pixel (Q_{min}=1), B is the minimum reflectance value, DN is the reflection value per pixel, and A is the value calculated by the following equation:

$$A = \frac{(L_{max} - L_{min})}{(Q_{max} - Q_{min})} \quad (3)$$

with L_{max} and L_{min} are the largest and smallest reflected values, respectively, and Q_{max} and Q_{min} are the largest (255) and smallest (1) quantised reflection values on the pixel cell, respectively.

For the Landsat 8 OLI:

$$L_\lambda = M_L \times DN + A_L \quad (4)$$

where M_L and A_L values are radiation multipliers and additions calculated for each channel, respectively.

The values L_{max} and L_{min}, Q_{max} and Q_{min}, and M_L and A_L are taken from an MTL file attached in the remote sensing image file when downloaded.

Conversion to reflection values: for the Landsat 5 TM:

$$\rho_p = \frac{\pi \times L_\lambda \times d^2}{ESUN_\lambda \times \cos\theta_s} \quad (5)$$

where ρ_p is the reflection value on the satellite corresponding with wavelength λ, L_λ is the radiation value on the satellite with unit $Wm^{-2}.\mu m^{-1}$, $ESUN_\lambda$ is the average lighting of the upper atmosphere from the Sun ($Wm^{-2}.Mm^{-1}$), θ_s is the angle of the sun's peak and the complementary angle of the Sun's elevation (θ_s = radians (90° - the angle of the Sun)) and *d* is the distance between Earth and Sun in astronomical units and calculated using Smith's equation (Eq. 6):

$$d = (1 - 0.01672 * \cos(\text{radians}(0.9856 * (\text{Julian Day} - 4)))) \quad (6)$$

with the Landsat 8 OLI, the reflectance value is calculated as the surface reflectance value with Eq. 7:

$$\rho = \frac{\pi * (L_\lambda - L_P) * d^2}{T_V * \{(ESUN_\lambda * \cos\theta_{SZ} * T_Z) + E_{down})\}} \quad (7)$$

with T_v and T_z being a function of transmitting atmospheric radiation from the Earth's surface to the receiver and from

the Sun to the Earth, respectively, $ESUN_\lambda$ is the average lighting of the upper atmosphere from the Sun ($Wm^{-2}Mm^{-1}$), E_{down} is the spectral radiation going to the object's terrain surface, *d* is the distance between the Earth and the Sun and L_P is the line radiation calculated by the following Eq. 8:

$$L_P = L_{min} - 0.01 * \frac{T_V * \{(ESUN_\lambda * \cos\theta_{SZ} * T_Z) + E_{down}\}}{\pi * d^2} \quad (8)$$

Based on the DOS method, the determination of T_V, T_Z, and E_{down} parameters which divided into many different methods (DOS1, DOS2, DOS3, DOS4) having different accuracy. In this study, the authors use DOS1, in which the parameters were determined by Moran and his team as T_V=1; T_Z=1; and E_{down} = 0. At this time Eq. 7 will become:

$$\rho = \frac{\pi * (L_\lambda - L_P) * d^2}{ESUN_\lambda * \cos\theta_{SZ}} \quad (9)$$

with L_p is calculated by Eq. 10:

$$L_P = L_{min} - 0.01 * \frac{ESUN_\lambda * \cos\theta_{SZ}}{\pi * d^2} \quad (10)$$

The algorithm calculates AOD

"Blur" effect: after radiation correction, the authors have an image showing the reflection value of the objects. Based on the results of the reflection, the authors proceed to extract AOD by the method of N. Sifakis and P-Y. Deschamps (1992) [14]. The team used 2 remote sensing images, one in completely clean air (used as a "reference image") and the other in polluted air for the survey. According to the previous study, surface radiation is a space-dependent variable and is not time based, so using differential textural analysis (DTA), the team extracted the approximate value of AOD [14].

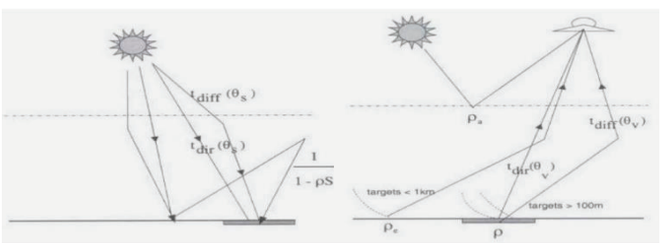

Fig. 3. Different components of total radiation transmitted up and down [14].

In the visible light spectrum of electromagnetic waves, the scattering of shortwave radiation is mostly caused by particulate matter in the atmosphere that causes a decrease in the contrast and distortion of the spectral feedback pattern in the remote sensing image (Fig. 3). This is called the "blurring" effect, which can be estimated using the optical depth (OD) derived from the basic equation of the apparent reflection from a satellite. For research objects in a large space (with a radius within 1 km) and homogeneity between different objects, the authors have the equation of "clear" reflection as follows:

$$\rho^* = \rho \frac{T(\theta_s)T(\theta_v)}{1-\rho S} + \rho_a \quad (11)$$

where ρ^*, ρ, and ρ_a are "clear" reflections in satellites, surface reflections, and atmospheric reflections, respectively. S is the spherical reflectance of the atmosphere defined as the ratio of scattering to total attenuation of radiation, θs and θv are the Sun's zenith angles and their zenith angles, respectively. $T(\theta_s)$ is the total transmission function on the "downlink", it can be analysed as the sum of $t_{dir}(\theta_s)$ and $t_{diff}(\theta_s)$ including direct and diffusion transfer functions. $T(\theta_v)$ is the total transmission function on the uplink and it can be analysed as the sum of $t_{dir}(\theta_v)$ and $t_{diff}(\theta_v)$ including direct and diffusion transfer functions. According to Eq. 11, the authors obtain information about optical thickness as a function of ρ_a with $\rho \approx 0$. However, for research areas having small diameters (<100 m), the authors need to consider the proximity effect and Eq. 1 needs to consider the average reflection of the surrounding objects (ρ_e). Then Eq. 11 will become:

$$\rho^* = \rho \frac{T(\theta_s)t_{dir}(\theta_v)}{1-\rho_e S} + \rho_e \rho \frac{T(\theta_s)t_{diff}(\theta_v)}{1-\rho_e S} + \rho_a \quad (12)$$

According to the authors, standard deviation is an indicator of similar contrast as seen on satellite images. So N. Sifakis and P-Y. Deschamps (1992) [14] have given the correlation equation between the standard deviation of the "clear" ($\sigma(\rho^*)$) reflectance and the standard deviation of the true reflectance ($\sigma(\rho)$) based on Eq. 12. The authors took a random set of adjacent pixel cells and found that the change of ($\sigma(\rho^*)$) is only affected by the standard deviation of the actual reflection at the surface ($\sigma(\rho)$). Therefore, the authors obtained the following correlation equation:

$$\sigma(\rho^*) = \sigma(\rho) \frac{T(\theta_s)t_{dir}(\theta_v)}{1-\rho S} \quad (13)$$

Appling the Lambert - Bouguer transmission law to the transmission function $t_{dir}(\theta_v)$, the authors calibrate it to the angle θ_v and the following equation is found:

$$\sigma(\rho^*) = \sigma(\rho) \frac{T(\theta_s)e^{-\tau/\cos(\theta_v)}}{1-\rho S} \quad (14)$$

According to Eq. 14, $-\tau/\cos(\theta_v)$ can be seen as AOD, which is calibrated to the Sun's angle.

Pixel: as mentioned above, following by the method of N. Sifakis and P-Y. Deschamps (1992) [14], the authors divide the study area into random pixel cells to calculate the reflectance standard deviation of the area.

AOD calculation: based on Eq. 14, the authors can calculate the standard deviation of the clean day and pollution day. Then, they take the equation for the clean day and divide by the pollution day, which yields the following equation:

$$\frac{\sigma_1(\rho^*)}{\sigma_2(\rho^*)} = \exp((-\tau_1/\cos(\theta_{v1}) + (-\tau_2/\cos(\theta_{v2})) \quad (15)$$

Landsat-8/OLI has zero viewing angles or zenith views at the center of the image. The maximum value of the view at the edges of the frame is 7.4960 calculated from the height of Landsat 8 satellite (703 km) and the width of 185 km. Hence the viewing angle range is from 0-7.4960 for any satellite image. For the Landsat 5 TM of the clean day image, the authors calculated the same zenith view from which the authors see that the clean day image angle ranged from 0-7.3950. Because the angle of view is small, the authors can assume that cos (θ_{v1}) ≈ cos (θ_{v2}) ≈ 1 and an error of ≈ 0.4%:

$$\frac{\sigma_1(\rho^*)}{\sigma_2(\rho^*)} = \exp(-\tau_1 - \tau_2) \quad (16)$$

with τ_1 and τ_2 is the atmospheric depth in the clean day and the pollution day, respectively. Based on Eq. 16, the authors calculate the AOD difference between the clean day and the pollution day as:

$$\Delta\tau = \tau_2 - \tau_1 = \ln[\frac{\sigma_1(\rho)}{\sigma_2(\rho)}] \quad (17)$$

In Eq. 17, the AOD is equal to the difference of optical depth in the clean and polluted images. However, for "clean days", the atmosphere is assumed to be completely "transparent" so it is possible to indicate that the optical depth on a clean day is approximately zero ($\tau_1 \approx 0$). So, from Eq. 17, the authors obtain the following equation:

$$\Delta\tau = \tau_2 = \ln[\frac{\sigma_1(\rho)}{\sigma_2(\rho)}] \quad (18)$$

The optical depth difference of the clean day and pollution day is also the optical depth of the pollution day and is determined by Eq. 18 [14-16].

Results

Correlation and regression analysis between real AOD and PM_{10}

Like most of the other studies on AOD determination as well as PM_{10} concentration distribution by remote sensing, this study conducted AOD surveys mainly on 4 spectral channels: the blue spectrum channel (0.450-0.515 μm), green spectrum channel (0.525-0.600 μm), red spectrum (0.630-0.680 μm), and near-infrared channel (0.845-0.885 μm). Table 1 shows the results obtained when extracting AOD from the 4 image channels.

Table 1. AOD extract results from 4 channels Landsat image.

Stations	PM_{10} concentration (μg/m³)	AOD in 28th Feb, 2017			
		Blue	*Green*	*Red*	*Near-infrared*
Zoo	66.4	-1.08318	-2.59237	-1.09258	-1.75548
Binh Chanh	138.5	-3.06638	-2.13509	-4.91728	-2.47673
DOSTE	112	-1.20462	-2.30867	-1.60878	-1.7548
Hong Bang	74.7	-2.04362	-3.58543	-2.67132	-1.14265
Thong Nhat Hospital	87	-2.04362	-3.78751	-1.92392	-2.33622
Tan Son Hoa	96.4	-1.99765	-3.91204	-2.05347	-1.45789
District 2	65	Noise	Noise	Noise	-2.67964

According to these results, the authors established scatter plots with AOD extracted as an independent variable (x) and the actual PM_{10} concentration as the dependent variable (y). Then, a regression equations was found and the results are given in Figs. 4-7.

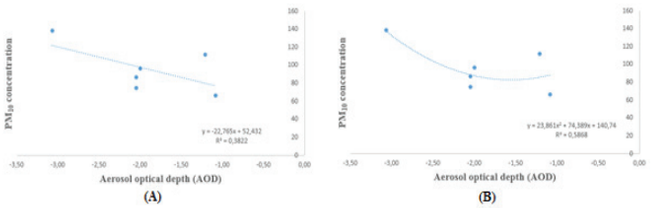

Fig. 4. The correlation between PM_{10} and AOD in the blue channel. (A) linear regression; **(B)** non-linear regression.

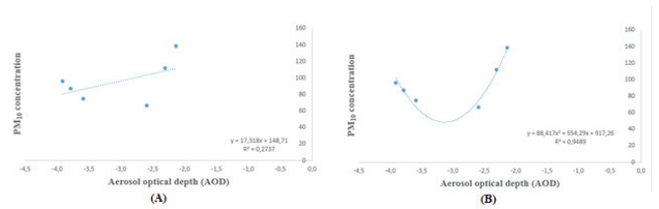

Fig. 5. The correlation between PM_{10} and AOD in the green channel. (A) linear regression; **(B)** non-linear regression.

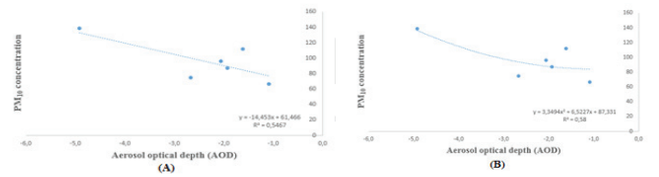

Fig. 6. The correlation between PM_{10} and AOD in the red channel. (A) linear regression; **(B)** non-linear regression.

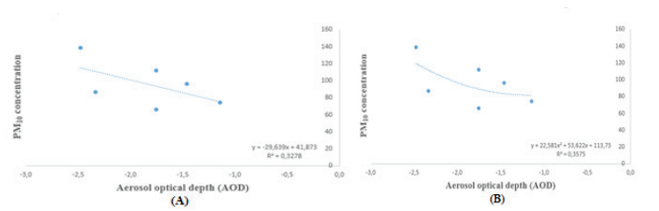

Fig. 7. The correlation between PM_{10} and AOD in the near-infrared channel. (A) linear regression; **(B)** non-linear regression.

Table 2. Regression analysis results among 4 image channels.

		Blue	Green	Red	Near-infrared
Linear regression equation	Equation	y=-22.8x + 52.4	y=17.3x + 148.7	y=-14.5x + 61.5	y=-8.1x + 75.6
	Correlation coefficients	R^2=0.3822	R^2=0.0223	R^2=0.5467	R^2=0.0299
Non-linear regression equation	Equation	y=23.8 x^2 +74.4x + 140.7	y=83.4x^2 +554.3x + 917.3	y=3.3 x^2 +6.5x+ 87.3	y=-32.9 x^2 - 135.9x - 38.9
	Correlation coefficients	R^2=0.5868	R^2=0.9489	R^2=0.58	R^2=0.1151

Through the analysis of the results (Table 2), the authors found that the non-linear regression equation of the blue spectrum channel gives the best correlation results between the two parameters (with R^2=0.9489). Therefore, the authors use non-linear regression between AOD and PM_{10} on the green channel [17].

Evaluation of the error between the actual measured dust concentration and the calculated dust concentration (Table 3)

Table 3. Assessment of the error between the actual measured concentration and the simulated concentration.

Station	Calculated PM_{10} concentration (µg/m^3)	Measured PM_{10} concentration (µg/m^3)	Absolute error
Zoo	66.4	41.9	24.5
Binh Chanh	138.5	124.1	14.4
DOSTE	112	102.2	9.8
Hong Bang	74.7	61.3	13.4
Thong Nhat Hospital	87	82.6	4.4
Tan Son Hoa	96.4	94.1	2.3
Error RMSE	13.5883		

Dust distribution map of Ho Chi Minh city area

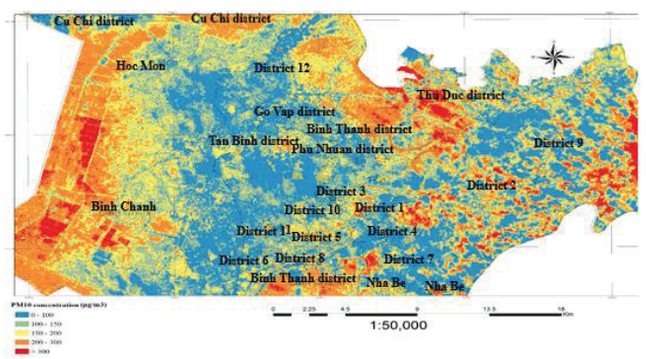

Fig. 8. Spatial concentration of PM_{10} in Ho Chi Minh city in February 28th, 2017.

The spatial concentration of the PM_{10} map was established in Ho Chi Minh city (Fig. 8). The map shows the concentration of dust in the area at 10 am, which is the time that vehicles and factories being operating. At this time, trucks are also allowed to run in the downtown area.

It can be seen that the PM_{10} concentration is highest, at over 300 µg/m^3, in districts with high traffic density and a concentration of many industrial parks such as Binh Chanh, Thu Duc, and district 9. Typically, in the area around the Thu Duc district, there are up to 150 factories with large production scale and thousands of small factories. Similarly, in the area around the Binh Chanh district, not only are there two large industrial parks Ho Chi Minh city, the Vinh Loc and Le Minh Xuan industrial parks, there are also many key roads such as the national highway 1A. High traffic volume also contributes to the high amount of dust and smoke in the Binh Chanh district compared to other areas.

In addition, Fig. 9 shows that PM_{10} concentration is distributed mainly in the western areas of the Hoc Mon and Binh Chanh districts and then disperses to surrounding areas. It can be understood that the process of dispersing suspended matter in the air is still influenced by the wind, but the inner city has a large surface roughness due to many high-rise buildings. So, a monsoon does not affect much in the inner city, only a "whirlwind" does. The characteristic of this wind is to blow along many directions under the influence of the moving flow of vehicles as well as the processes of heat emission from human activities.

In order to consider changes in PM_{10} concentration over time, the authors use the correlation equation obtained over a number of years between 2009-2019. The years selected for the analysis are selected according to the following criteria: photos are available in February each year; selected images with little cloud cover; in the period of 10 years between 2009-2019.

Based on the above criteria, the authors choose 4 years including February 11th, 2010, February 9th, 2015, February 28th, 2016, and February 17th, 2018. The authors obtained the research results shown in Fig. 9.

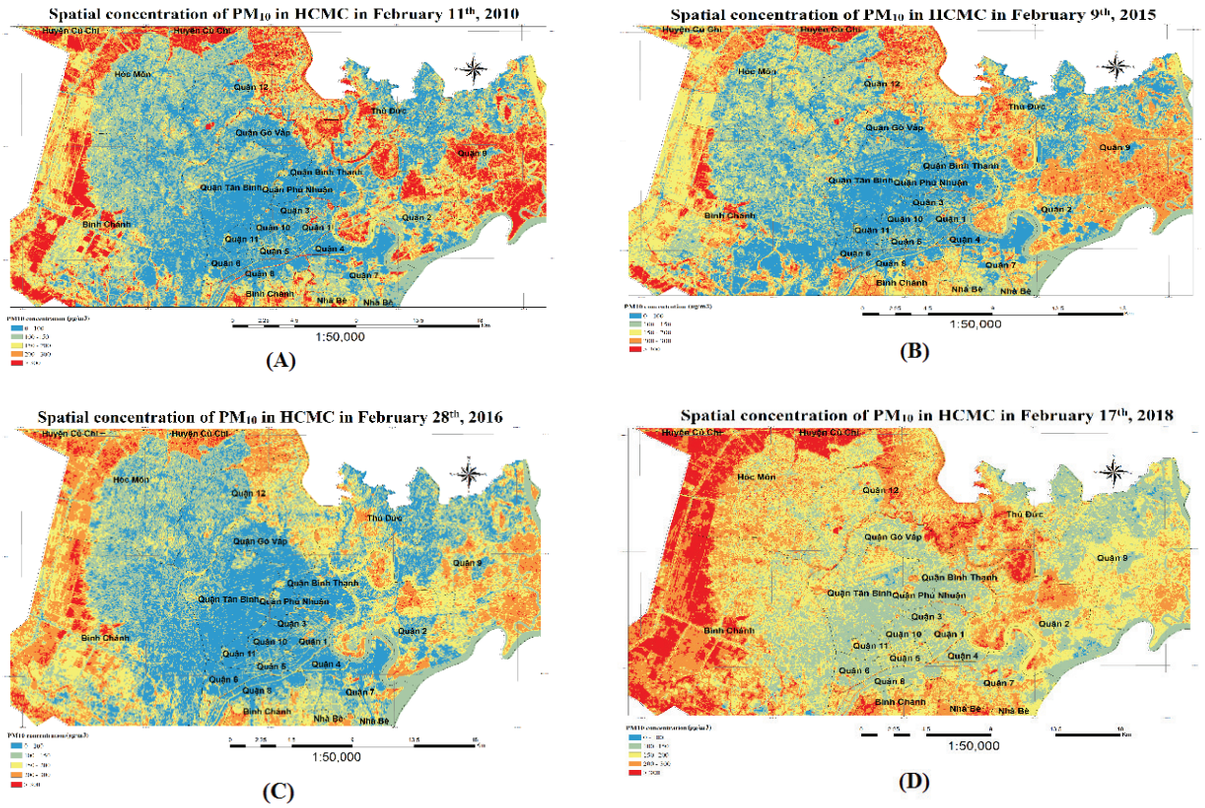

Fig. 9. Spatial concentration of PM_{10} in Ho Chi Minh city in (A) February 11th, 2010; (B) February 9th, 2015; (C) February 28th, 2016; (D) February 17th, 2018.

The results show that PM_{10} concentration in Ho Chi Minh city has increased over time (2010>2016>2015>2017>2018) and there is a fluctuation in concentration across the region. It can be seen that dust movements in the study area fluctuate equally over the years and the highest PM_{10} concentration is in the suburbs of the city. In central Ho Chi Minh city, PM_{10} concentrations increase over the years, especially along major regional roads. In addition, PM_{10} concentration increased sharply in the area of Binh Chanh, Thu Duc, and district 2 due to the strong development of industrial activities. Over time, large and small production factories and industrial zones are growing more and more. Consequently, the transport and transportation activities on route 2 of this area also increased. Particularly in district 2, there is the Cat Lat port that is adjacent to the Hanoi highway with dense traffic between these two areas.

Conclusions

The objective of the study is to use PM_{10} monitoring data in real time together with satellite image data analysis to give an equation showing the relationship between AOD and actual measured PM_{10} concentration. The final result provides an overview of the distribution of pollution concentration in the study area and dust concentration mainly in areas with high traffic density and dense industrial areas like the Binh Chanh,Thu Duc districts, and district 2 with dust concentrations of >300 $\mu g/m^3$. In the remaining areas, the dust concentration is uneven in the range of 50-200 $\mu g/m^3$. At the same time, this work also helps to increase reliability in the application of remote sensing methods for air quality monitoring. Compared to ground monitoring methods, the authors of this work only know the environmental status at the measured location so a wide area cannot be assessed. With the modelling method, the results are also limited due to rather complex input requirements (meteorology, emission sources, etc.). Therefore, using remote sensing technology to create pollution maps for environmental management will bring more efficiency.

Currently, the monitoring stations in the area of Ho Chi Minh city are mainly located in urban areas, so the assessment of air quality is still limited. However, the construction of additional monitoring stations is quite costly, so the assessment of air quality by satellite images is more economical thanks to the advantages of being able to obtain large-scale data together. With the treatment and calculation methods that have been tested in many studies

around the world over the years, the remote sensing method can be added as a useful tool for monitoring and evaluating air pollution in the city.

COMPETING INTERESTS

The authors declare that there is no conflict of interest regarding the publication of this article.

REFERENCES

[1] Ministry of Natural Resources and Environment (2016), *National Environmental Status Report 2016: Urban Environment*, Vietnam Publishing House of Natural Resources, Environment and Cartography, **2**, pp.25-45, in Vietnamese.

[2] https://www.who.int/docs/default-source/gho-documents/health-in-2015-mdgs-to-sdgs/health-in-2015-from-mdgs-to-sdgs.pdf?sfvrsn=8ba61059_2.

[3] https://www.who.int/docs/default-source/gho-documents/world-health-statistic-reports/world-heatlth-statistics-2016.pdf.

[4] Tran Thi Van, et al. (2014), "Remote sensing optical thickness aerosol simulation of PM_{10} distribution in urban areas of Ho Chi Minh city", *VNU Journal of Science*, **30(2)**, pp.52-62.

[5] Nguyen Nhu Hung, et al. (2018), "Model to determine PM_{10} dust in Hanoi area using Landsat 8 OLI satellite image data and visual data", *VNU Journal of Science*, **34(1)**, pp.23-36, in Vietnamese.

[6] A.R. Huete (2004), "Remote sensing for environmental monitoring", *Environmental Monitoring and Characterization*, pp.183-206.

[7] S.K. Satheesh (2002), "Aerosol and climate", *Resonance - Journal of Science Education*, **7(4)**, pp.48-59.

[8] K. Omari, et al. (2019), "Aerosol optical depth retrieval over the city of Abu Dhabi, United Arab Emirates (UAE) using Landsat-8 OLI images", *Atmospheric Pollution Research,* **10(4)**, pp.1075-1083.

[9] Tran Thi Van, et al. (2012). "Study the possibility of detecting dust pollution in urban areas by remote sensing technology", *Science and Technology Development Journal*, **15(M2-2012)**, pp.33-47, in Vietnamese.

[10] L. Sun, et al. (2016), "Aerosol optical depth retrieval over bright areas using Landsat 8 OLI images", *Remote Sensing*, **8(1)**, 23pp.

[11] N. Othman, et al. (2010), "Estimating particulate matter concentration over arid region using satellite remote sensing: a case study in Makkah, Saudi Arabia", *Modern Applied Science*, **4(11)**, pp.131-142.

[12] K. Zanter (2015), "Conversion of DNs to physical units", *Landsat 8 Data Users Handbook 1st version*, U.S Geological Survey, pp.61-65.

[13] K. Zanter (2019), "IGS Landsat data archives", *Landsat 7 Data Users Handbook*, U.S Geological Survey, pp.107-127.

[14] N. Sifakis, P-Y. Deschamps (1992), "Mapping of air pollution using SPOT satellite data", *Photogrammetric Engineering and Remote Sensing*, **58(10)**, pp.1433-1437.

[15] A. Retalis, et al. (1999), "Assessment of the distribution of aerosols in the area of Athens with the use of Landsat thematic mapper data", *Int. J. Remote Sensing*, **20(5)**, pp.939-945.

[16] W.E.K. Middleton (1961), *Pierre Bouguer's Optical Treatise on Gradation of Light*, University of Toronto Press, 265pp.

[17] Nguyen Tran Que, Vu Manh Ha (2008), *Textbook of Economic Statistics*, Hanoi National University Publishing House, 208pp, in Vietnamese.